


Cite this: *RSC Adv.*, 2024, 14, 33512

An elegant approach for the synthesis of multisubstituted imidazole *via* FeCl₃/SiO₂ catalyzed activation of acetals: a photophysical study of an imidazole–carbazole hybrid†

Barnali Das,^a Arghyadeep Bhattacharyya,^a Bhaswati Paul,^b Ramalingam Natarajan^b and Swapan Majumdar^{*a}

A simple and solvent-free catalytic system was developed for the direct conversion of multisubstituted imidazoles through the reaction of acetals and benzils with ammonium acetate/amines as the source of nitrogen. The reaction occurred under mild and benign conditions using FeCl₃/SiO₂ as a heterogeneous catalyst without the requirement of any toxic organic solvents. The easy preparation and recyclability of the catalyst allows the reaction to be simple and highly efficient, resulting in very good yields of imidazoles. Novel imidazole–carbazole hybrid compounds were also synthesised by adopting the present methodology. Single crystal X-ray diffraction study indicated the presence of a CH⋯π supramolecular interaction that renders effective molecular packing in the solid state. The steady-state and spectro-dynamic behaviours of these hybrid molecules were investigated, and it was revealed that a solvent-dependent excimer-coupled ICT phenomenon guided excited state photophysics. Very unusual excimer lifetime was noticed in the solid state of this bis-heterocyclic compound owing to the stacking of molecules *via* CH⋯π interaction, as evident from the X-ray studies.

Received 6th September 2024
Accepted 8th October 2024

DOI: 10.1039/d4ra06436d

rsc.li/rsc-advances

Introduction

The ideation for the synthesis of various unique heterocyclic compounds is of keen interest to organic and medicinal chemistry researchers because of their various applications in pharmaceutical chemistry, drug industry and many other areas of science.^{1,2} Imidazoles are a vital class of nitrogen-containing heterocycles that are present in numerous bioactive molecules and possess known biological and pharmacological activities,^{3–8} such as anti-obesity, anti-hypertension, anti-allergic, anti-inflammatory, anti-bacterial, anti-viral, anti-tumor, analgesic, anti-histaminic, anti-helminthic, anti-thyroid, and anti-ulcer activity. Furthermore, they have high versatile utility in other areas such as dyes for solar cells,⁹ agrochemicals,¹⁰ optical applications,¹¹ functional materials,¹² plant growth regulators, fungicides and herbicides.¹³ Some substituted imidazoles are selective antagonists of the glucagon receptors and inhibitors of IL-1 biosynthesis.¹⁴ Moreover, the imidazole nucleus constitutes the core unit of many natural products,¹⁵ such as histidine,

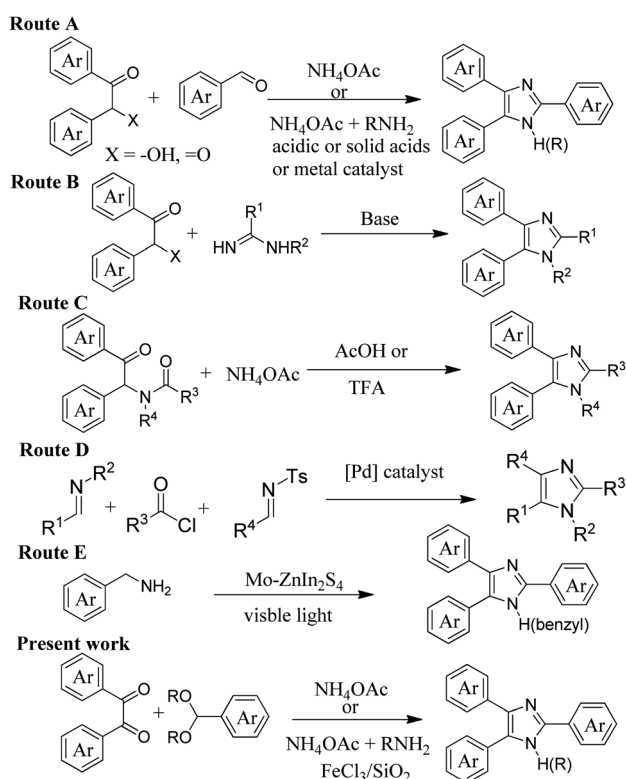
histamine, biotin, and pilocarpine. Moreover, 2,4,5-triaryl imidazoles are popular building blocks for the construction of pharmaceutically interesting compounds, such as inhibitors of p38 MAP kinase¹⁶ and B-Raf kinase transforming growth factor b1,¹⁷ and are the core structural skeleton of several drugs, such as trifluenagrel, eprosartan, and losartan.¹⁸ Substituted imidazoles also have important applications in the chemistry of functional materials, such as in functional polymers,¹⁹ ligands,²⁰ photo-physical materials,^{21,22} ionic liquids,²³ semiconductor devices,²⁴ fluorescent probes,²⁵ and N-heterocyclic carbenes.²⁶ Hybrid molecules are chemical entities that have two or more structural domains with different functional roles and show dual activities in the biological function and modulation of functional materials. Hybrid molecules have the potential to minimize toxicity, widen the biological range, overcome drug cross-resistance, and improve efficacy as compared to the parent drugs. In recent years, covalently linked different functionalized heterocyclic units as the so-called organic–organic hybrid have emerged as a powerful tool for the modulation of their physical and electronic properties.²⁷ Functional modification offers a direct and robust method for tuning their physicochemical properties in a controlled and modular manner. This is particularly important as the rational design of species with well-defined electronic properties remains a key target for both biological and photochemical applications.²⁸ In this context, an imidazole–carbazole hybrid has

^aDepartment of Chemistry, Tripura University, Suryamaninagar, 799 022, India. E-mail: smajumdar@tripurauniv.ac.in; Fax: +91-381-2374802; Tel: +91-381-237-9070

^bCSIR-Indian Institute of Chemical Biology, 4, Raja S. C. Mullick Road, Kolkata 700 032, India

† Electronic supplementary information (ESI) available. CCDC 2361185. For ESI and crystallographic data in CIF or other electronic format see DOI: <https://doi.org/10.1039/d4ra06436d>


attracted attention from chemists because of its bipolar D- π -A type transition for blue light-emitting diodes²⁹ and electrochemical sensors.³⁰ Consequently, the development of novel synthetic methods for the synthesis of diverse structured imidazoles has attracted sustained interest in organic synthesis. The tri- and tetra-substituted imidazoles can be synthesized by the reaction of a 1,2-diketone/ α -hydroxy ketone with an aldehyde and ammonium acetate and/or primary amines under acidic condition,^{31–35} microwave reactor,³⁶ and using different heterogeneous metal catalysts (Scheme 1, route A).^{37–40} Other approaches like the reaction of α -haloketone with a substituted amidine^{10,11,41} (Scheme 1, route B) or the cyclocondensation of *N*-alkyl- α -acetamido ketone/alcohol with ammonium acetate in HOAc under reflux⁴² (Scheme 1, route C), or by the condensation of imines and acyl chloride over a palladium catalyst (Scheme 1, route D)⁴³ have been reported for the synthesis of multi-substituted imidazoles. Recently, the visible light-induced photo-cyclization of amines to imidazoles *via* C-C/C-N bond coupling, followed by dehydrogenation reaction over Mo-doped ZnIn₂S₄ as a heterogeneous photocatalyst was also reported (Scheme 1, route E).⁴⁴ Although there are various ways to synthesize imidazoles (Scheme 1), some of the catalysts possess objectionable drawbacks from the view point of environment and green chemistry. Thus, the development of a new and simple strategy is still desirable for the direct construction of poly-substituted imidazoles with more economic viability and sustainability.

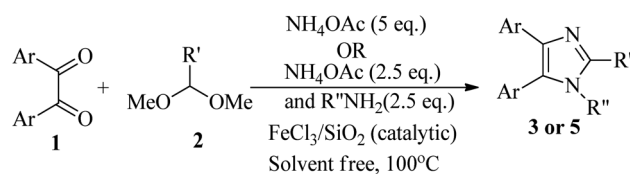


Scheme 1 Different routes towards the synthesis of substituted imidazoles.

Nowadays, solid-supported reagents using polystyrene-based resin and silica gel as the scavenger are gaining increasing attention due to several advantages associated with them. However, silica gel has been widely accepted since it is less expensive and structurally rigid with high mechanical and thermal stability. Silica gel also does not swell in any organic solvents. Thus, it can be used in various reaction media. Most importantly, silica gel has a large surface area (typically 200–800 m² g^{−1}), which allows for a high density of functional groups to be immobilized on its surface.⁴⁵ Due to the Lewis acid character of iron(III) chloride, it is extensively used in organic synthesis as a catalyst/activator since it is also inexpensive and readily available. However, this reagent cannot be recycled after its use, which ultimately creates pollution problems. By considering the aforementioned features of the supported reagents as a heterogeneous catalyst, we have successfully utilized silica-supported ferric chloride (FeCl₃/SiO₂) as an activator for various functional groups and in various occasions.^{46,47} It was reported that the acetal group can be activated by ferric chloride⁴⁸ or other transition metal catalysts⁴⁹ for the synthesis of heterocycles and other purposes under mild condition. Based on the above fact, we were curious to explore whether such activation could be applied to the synthesis of multisubstituted imidazoles using acetal as latent aldehydes under the FeCl₃/SiO₂ catalytic condition. Thus, we report herein our findings on to the synthesis of 2,4,5-tri and 1,2,4,5-tetra substituted imidazoles in the presence of a silica-supported FeCl₃/SiO₂ catalyst under solvent-free condition using different protected acetals as the source of the C-2 carbon (Scheme 2). Due to the structural uniqueness of one of the synthesized multisubstituted imidazole-carbazole hybrid compounds, we also demonstrated its solid state packing pattern and photo-physical behaviour in this communication.

Results and discussion

Based on our previous experience,³² we have decided to begin with Amberlite IR 120 H+ as the catalyst to optimize the best reaction condition to achieve maximum yield of the product. So, we begin by reacting benzil (**1a**; 1 mmol) with benzaldehyde dimethyl acetal (**2a**; 1.1 mmol), ammonium acetate (5.0 mmol), and Amberlite IR 120 H+ (30 mg) in methanol at room temperature. No reaction was detected on a TLC plate (Table 1, entry 1). However, upon refluxing the mixture for 3 h in methanol or ethanol, 2,4,5-triphenyl imidazole was obtained in 65% yield from the reaction mixture after purification (Table 1, entries 2 and 3). Surprisingly, when the reaction was carried



Scheme 2 General reaction scheme for the synthesis of substituted imidazoles.

Table 1 Optimization of the reaction conditions for the formation of 2,4,5-triphenylimidazole from benzil and benzaldehyde dimethylacetal via a domino multicomponent reaction

Reaction scheme: Benzil (1a, 1 mmol) + Benzaldehyde dimethylacetal (2a, 1.1 mmol) $\xrightarrow[\text{Condition Table 1}]{\text{NH}_4\text{OAc}}$ 2,4,5-triphenylimidazole (3a)

Entry	Solvent	Catalyst	NH ₄ OAc	Temp. (°C)	Time (h)	Yield (%)
1	MeOH	Amberlite IR 120 H ⁺ (30 mg)	5.0 eq.	rt	3.0	NR
2	MeOH	Amberlite IR 120 H ⁺ (30 mg)	5.0 eq.	Reflux	3.0	65
3	EtOH	Amberlite IR 120 H ⁺ (30 mg)	5.0 eq.	Reflux	180	65
4	MeOH (dry)	Amberlite IR 120 H ⁺ (30 mg)	5.0 eq.	Reflux	3.0	Trace
5	THF (dry)	Amberlite IR 120 H ⁺ (30 mg)	5.0 eq.	rt	3.0	NR
6	MeOH	None	5.0 eq.	Reflux	3.0	NR
7	No	Amberlite IR 120 H ⁺ (30 mg)	5.0 eq.	80 °C	3.0	Trace
8	MeOH	Amberlyst 15 (30 mg)	5.0 eq.	Reflux	1.0	57
9	CH ₂ Cl ₂	FeCl ₃ (20 mg)	5.0 eq.	Reflux	1.0	Mixture
10	MeOH	FeCl ₃ /SiO ₂ (20 mg)	5.0 eq.	Reflux	1.0	Mixture
11	EtOH	FeCl ₃ /SiO ₂ (20 mg)	5.0 eq.	Reflux	3.0	Mixture
12	No	FeCl₃/SiO₂ (20 mg)	5.0 eq.	100 °C	1.0	93 (ref. 32)
13	No	FeCl ₃ /SiO ₂ (20 mg)	5.0 eq.	80 °C	1.0	Mixture
14	No	FeCl ₃ /SiO ₂ (20 mg)	5.0 eq.	100 °C	4.0	94
15	No	FeCl ₃ /SiO ₂ (50 mg)	5.0 eq.	100 °C	1.0	94
16	No	Silica-gel (230–400 mesh)	5.0 eq.	100 °C	1.0	Mixture
17	No	FeCl ₃ /SiO ₂ (10 mg)	5.0 eq.	100 °C	4.0	85
18	No	FeCl ₃ /SiO ₂ (20 mg)	1.0 eq.	100 °C	1.0	Mixture
19	No	FeCl ₃ /SiO ₂ (20 mg)	2.0 eq.	100 °C	1.0	65
20	No	FeCl ₃ /SiO ₂ (20 mg)	10.0 eq.	100 °C	1.0	93
21	No	FeCl ₃ /SiO ₂ (20 mg)	5.0 eq.	100 °C	1.0	93, 92, 92, 90, 89

using dry methanol or THF, or without catalyst or solvent, by keeping the ratios of the reactants the same, no product was detected (entries 4–6). The reaction is also unsatisfactory for the catalyst Amberlyst 15 under identical conditions (entry 8). Having in mind the Lewis acidic nature of FeCl₃, we then turned our attention toward its use as an activator for acetals. Accordingly, we have employed a catalytic amount of anhydrous ferric chloride (20 mg mmol⁻¹) in dichloromethane at room temperature, but such attempt resulted in a mixture of products (Table 1, entry 9), along with unreacted benzil. Refluxing the reaction mixture in methanol/ethanol in the presence of silica-supported ferric chloride (20 mg, 2 mol% of FeCl₃) resulted in an incomplete conversion to products (Table 1, entries 10 and 11). However, one of the products was identified as 2,4,5-triphenyl imidazole on a TLC plate by the comparison of the standard sample. Then, we were curious to see the outcome of the reaction under solvent-free conditions. Accordingly, a mixture of **1a** (1 mmol) with **2a** (1.1 mmol) and ammonium acetate (5 mmol) and FeCl₃/SiO₂ (20 mg) was heated without the use of any solvent for 1 h at 100 °C. Under this condition, a clean conversion occurred and 93% yield of 2,4,5-triphenyl imidazole (**3a**) was isolated after work-up (Table 1, entry 12). Decreasing the temperature to 80 °C again showed incompatibility of the process (Table 1, entry 13). From this promising result, extending the reaction time to 4.0 h or increasing the amount of supported catalyst only had a slight influence on the yield (Table 1, entries 14 and 15). To gain further insight into the reaction system, control experiments were conducted in the

presence of silica-gel only. However, no product was detected (Table 1, entry 16). Decreasing the amount of the catalyst (10 mg), while keeping the others constant, resulted in a decreased yield of the tri-substituted imidazole (Table 1, entry 17). An exhaustive literature search revealed that different synthetic procedures employed variable amounts of ammonium acetate, depending on the reaction conditions, to produce the desired product in maximum yield. Thus, to complete our optimization study, we also employed variable amounts of ammonium acetate. However, considerably lower yields were obtained when 1 and 2 equivalents were used, and the use of 10 equivalents does not affect the yield of 2,4,5-tri phenyl imidazole (Table 1, entries 18–20). We also found that the catalyst can be recycled through at least five consecutive cycles without the loss of catalytic potency (93% initial, 92%, 92%, 90% and 89%) of FeCl₃/SiO₂ (Table 1, entry 21).

We then turned our attention to the expansion of the sources of nitrogen by replacing ammonium acetate with other ammonium salts like ammonium chloride, ammonium formate, ammonium nitrate and ammonium sulphate. However, our study revealed that NH₄OAc is best, and the only effective source of nitrogen in the present method of imidazole synthesis (results not shown). Therefore, the conditions described in Table 1, entry 12 using benzil/benzaldehyde dimethylacetal/ammonium acetate in a molar ratio of 1 : 1.1 : 5 were found to be optimal, allowing for maximum conversion into the desired product **3a**. With the optimal reaction condition in hand, the scope of the devised system was evaluated by



varying the substituted benzils and acetals (Table 2). Acetals of aromatic aldehydes substituted with either electron-donating (**2b**) or electron-withdrawing (**2c**) functional groups in the *para* position reacted smoothly with **1a** and 5 eq. of ammonium acetate to provide the corresponding 2,4,5-triarylimidazoles **3b–c** in excellent yields (90% and 92%, respectively) (Table 3, entries 1 and 2). The presence of the $-\text{NO}_2$ group in acetal makes the process a little slower. 4,4'-Dimethoxy benzil (**1b**) also reacts

with both the benzaldehyde dimethyl acetal or 4-methoxy benzaldehyde dimethyl acetal under identical conditions to produce the corresponding triaryl imidazoles **3d–e** in excellent yields. To expand the scope of our methodology, cyclic-1,2-dione, *e.g.*, phenanthroquinone (**1c**), was evaluated for the present strategy, and also furnished the expected imidazoles **3f–g** in high yields. Next, reactions of benzaldehyde dimethyl acetals with butane 2,3-dione or cyclohexa-1,2-diones were

Table 2 Scope of the $\text{SiO}_2/\text{FeCl}_3$ -catalysed synthesis of trisubstituted imidazoles using NH_4OAc as the source of nitrogen

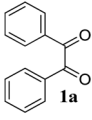
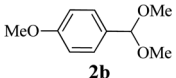
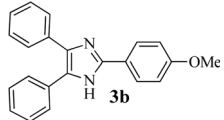
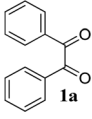
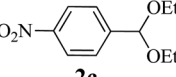
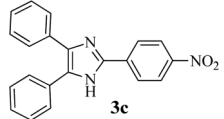
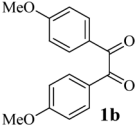
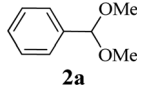
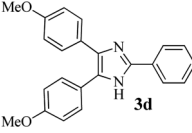
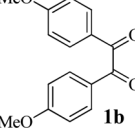
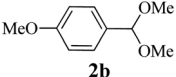
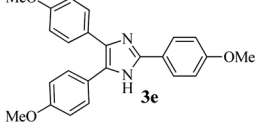
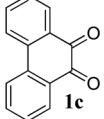
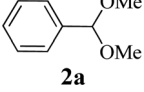
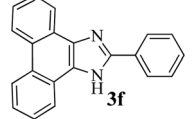
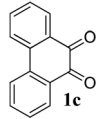
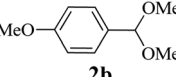
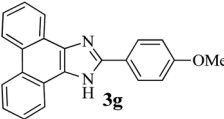
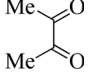
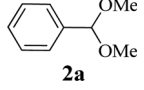
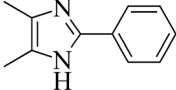
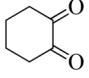
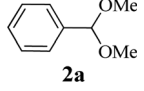
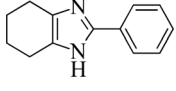
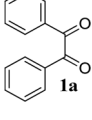
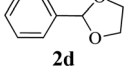
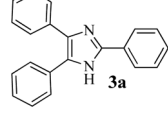
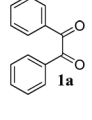
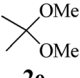
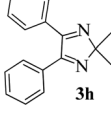
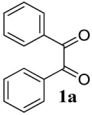
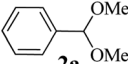
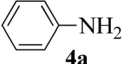
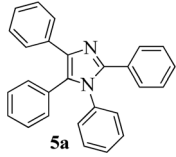
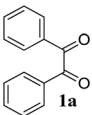
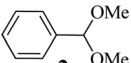
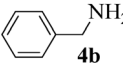
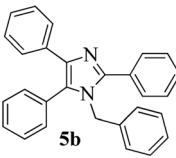
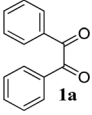
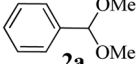
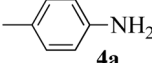
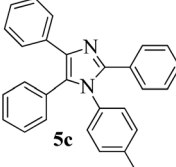
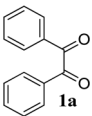
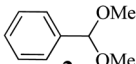
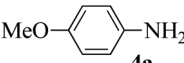
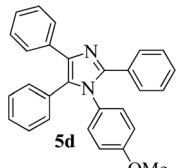
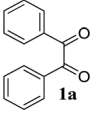
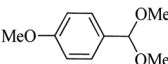
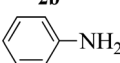
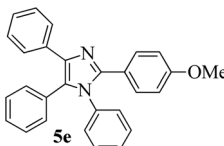
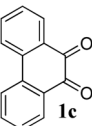
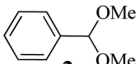
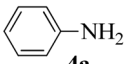
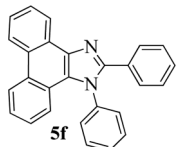
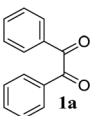
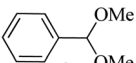
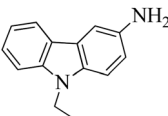
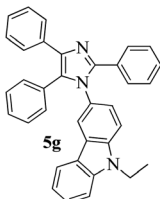
Entry	1,2-Dicarbonyl	Acetal	Product	Time (h)	Yield (%)
1	 1a	 2b	 3b	60	90 (ref. 32)
2	 1a	 2c	 3c	120	92 (ref. 32)
3	 1b	 2a	 3d	60	90
4	 1b	 2b	 3e	90	87
5	 1c	 2a	 3f	90	90 (ref. 50)
6	 1c	 2b	 3g	120	88 (ref. 51)
7	 1d	 2a	 3h	60	NR
8	 1e	 2a	 3i	60	NR
9	 1a	 2d	 3a	60	90 (ref. 32)
10	 1a	 2e	 3h	60	80



Table 3 Solvent-free synthesis of 1,2,4,5-tetrasubstituted imidazoles through a MCR of diketone, protected aldehydes, NH_4OAc , and amine using the $\text{FeCl}_3/\text{SiO}_2$ catalyst

Entry	1,2-Dicarbonyl	Acetal and amine	Product	Time (min)	Yield (%)
1		 		60	91 (ref. 32)
2		 		60	93 (ref. 32)
3		 		90	89 (ref. 52)
4		 		90	85 (ref. 53)
5		 		90	82 (ref. 54)
6		 		120	86
7		 		140	82

investigated. Unfortunately, such attempts were not compatible with this transformation, even though various reaction conditions were tried. To further evaluate the scope of the developed system, cyclic acetal (**2d**) was used in the same reaction with benzil, and an almost comparable yield of triaryl imidazole **3a** was observed. We have also extended our study with the ketal generated from acetone (**2e**) under standardized condition (Table 1, entry 12), and the expected 2,2-dimethyl-4,5-diphenyl-2H-imidazole (**3h**) was isolated in 80% yield after 1 h.

Based on the optimized reaction conditions, we have also devised the protocol for the synthesis of 1,2,4,5-tetrasubstituted imidazoles (**5**) using ammonium acetate, along with primary amines (**4**) as the source of the second nitrogen. Thus, we performed the synthesis *via* four-component, one-pot condensation of benzils (**1**), acetal (**2**), NH_4OAc and primary amines (**4**) in the presence of $\text{FeCl}_3/\text{SiO}_2$ under the standardized condition (Table 1, entry 12). Both aromatic and aliphatic primary amines furnished tetra-substituted imidazoles in excellent yield (82–



93%). Benzylamine provided better yield (**5b**, 93%) than aniline (**5a**, 91%) because of its better nucleophilicity. In the case of *p*-toluidine and *p*-methoxy aniline, the reaction proceeded efficiently under solvent-free conditions, and 1,2,4,5-tetrasubstituted imidazoles **5c–d** were produced in high yields. 4-Methoxy benzaldehyde dimethyl acetal also participated in the reaction with benzil, aniline and ammonium acetate to yield tetrasubstituted imidazole **5e** in 82% yield. However, phenanthroquinone reacted with benzaldehyde dimethyl acetal, aniline and ammonium acetate to yield the phenanthrene-fused imidazole derivative **5f** in 86% yield. Finally, we have achieved a very interesting synthesis of imidazole–carbazole hybrid compounds *via* the present four-component protocol using benzil, benzaldehyde dimethylacetal, ammonium acetate and 9-ethyl-3-amino carbazole under the standardized condition, and the hybrid compound **5g** was formed in 82% yield after 2.5 h. The structural uniqueness of **5g** containing two heterocyclic units could lead to novel photo-physical and optoelectronic properties, apart from the expected intramolecular charge transfer (ICT) commonly shown in carbazole and imidazole moieties separately. The single crystal X-ray analysis provides valuable information on the supramolecular interactions, which could in turn dictate their optoelectronic properties. Thus, we were also interested to see the solid-state structure of **5g** by X-ray diffraction studies, as the compound is found to be a highly crystalline solid. For this, single crystals were grown in a methanol–water solvent system to obtain suitable ones for analysis. Fig. 1(A) shows the ORTEP diagram of **5g** (CCDC deposition number 2361185) at 60% probability of the thermal ellipsoids, whereas Fig. 1(B) shows the packing of two molecules of **5g** in a unit cell. As **5g** comprises considerable π electron density, non-classical supramolecular interactions were also expected to be present *via* non-classical hydrogen bonding interactions. Fig. 1(C) and (D) illustrate the supramolecular architecture attained in **5g**. In Fig. 1(C), the presence of non-classical $\text{CH}\cdots\pi$ hydrogen bonding interactions ($d_{\text{H}\cdots\text{A}} \geq 2.0 \text{ \AA}$) could be visualized. Fig. 1(D) shows how the cumulative result of all such interactions leads to knitting a beautiful zig-zag assembly that extends in three dimensions.

Photo-physical study of imidazole–carbazole hybrid **5g**

The design of molecular frameworks to purposefully tune intriguing photo-physical phenomena, such as excited state proton transfer (ESIPT), excited state intramolecular charge transfer (ESICT), excimer formation, among others, has attracted the attention of chemists for a long time, owing to their multifarious utilities in the fields of sensing, bio-imaging and organic electronics.^{55–57} In this connection, the spectroscopic properties of the new compound **5g** (Table 3, entry 7) were investigated. The rationale behind choosing the same was the unique unison of carbazole, as well as imidazole units, both being very well-studied fluorophore units individually. However, the structural uniqueness of the conjugation of the two units could lead to novel spectroscopic properties apart from the expected intramolecular charge transfer (ICT) commonly shown in carbazole and imidazole moieties

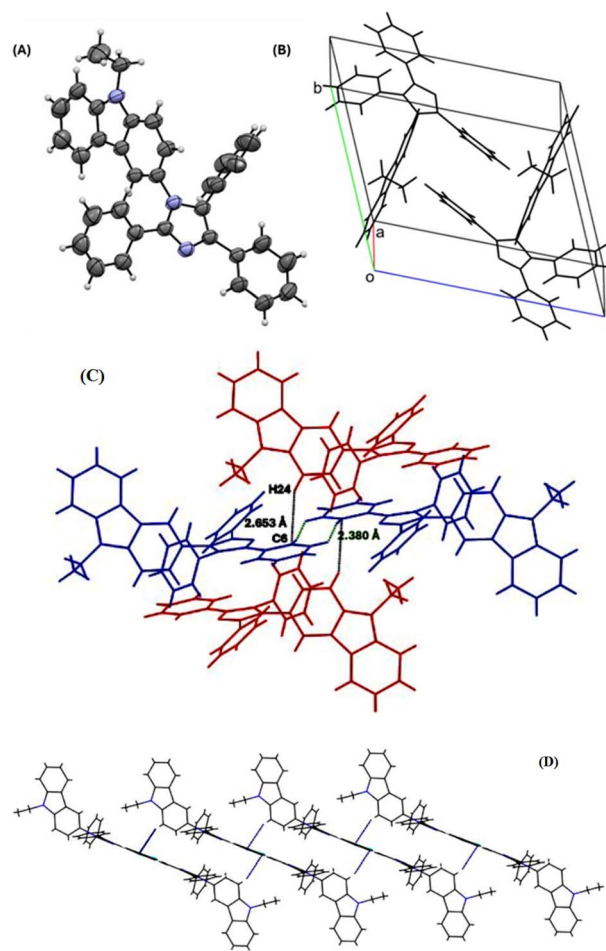


Fig. 1 (A) ORTEP diagram of **5g**. (B) Unit cell packing of **5g**. (C) Non-classical hydrogen bonding interaction between three units of **5g**. (D) Supramolecular architecture attained by the $\text{C-H}\cdots\pi$ interactions among individual units of **5g**.

separately. To our delight, **5g** showed rare excimer-based emission, a phenomenon observed predominantly in molecular entities like naphthalene, pyrene and perylene. The excimer emission band appeared as a broad, red-shifted band emitting at $\lambda_{\text{em}} \geq 400 \text{ nm}$ ($\lambda_{\text{ex}} 300 \text{ nm}$) depending on the solvent in the steady state emission profile, whereas the time-resolved emission decays consisted of abnormally high lifetime values (6.0–12.0 ns), accompanied with a growth component ($\tau_{\text{growth}} = 0.20\text{--}0.70 \text{ ns}$) in polar solvents, thereby providing solid support in favor of excimer emission. In addition, in chloroform, evidence of a feeble ESIPT could be obtained from the combined steady-state and time-resolved experiments. However, the solid-state emission was guided exclusively by monomer and excimer emission, without involvement of an ESIPT ($\tau_{\text{excimer}} = 17.0 \text{ ns}$). To our knowledge, this is the first report demonstrating a carbazole-substituted imidazole-enabled excimer emission, along with weak ESIPT, depending on the solvent polarity and viscosity. Prior to the current report, excimer formation was observed in some triphenylamine- and pyrrole-conjugated carbazole derivatives, albeit the spectro-dynamic properties were not explored.^{58,59} In the current

report, the detailed spectro-dynamic studies and steady-state experiments make it an improvement over the existing reports. The simple design yet elegant spectroscopic features of **5g** shall act as a guideline for unravelling the excited state photo-physical phenomena in the tailor-made carbazole-imidazole hybrid fluorophores. All steady-state and time-resolved measurements in solution were performed by using 15 μM solutions of **5g** (purity > 99.99%; HPLC, ESI) prepared in various solvents of differing polarity, proticity, and viscosity (*viz.*, chloroform, tetrahydrofuran, dimethylformamide, methanol and water of pH 7.0). For measurements in aqueous solution, the stock solution of **5g** in THF was diluted in water (pH 7.0) to get a final concentration of 15 μM . For solids, a morsel of powdered **5g** was smeared on a 1 cm \times 2 cm Whatman 40 filter paper strip using a spatula, and the filter paper coated with **5g** was used for spectroscopic measurements. The radiation areas of the emission spectrophotometer, as well as the nano-LED, were much lower than the area of **5g** smeared on the filter paper, ensuring no scattering from the filter paper.

Steady-state spectral features in solution and solid phase

To begin with, the steady-state spectra of **5g** were recorded in solution ($[\text{5g}] = 15 \mu\text{M}$), as well as in the solid phase (powdered form) (Fig. 2). The spectral features in the solution phase shall be discussed first, followed by that of the solid phase. Table 4 lists the important spectral data of **5g** in various solvents. From Fig. 2(A), it could be found that **5g** shows a structured absorption band centred at $\sim 300 \text{ nm}$, along with a very weak band at $\sim 360 \text{ nm}$. The high-energy band could be assigned to the $\pi \rightarrow \pi^*$ transition, which is in line with reported carbazole based molecules.^{60,61} The low-energy band can be assigned to the $n \rightarrow \pi^*$ transition, owing to the extremely low extinction coefficient ($\epsilon_{300 \text{ nm}} : \epsilon_{400 \text{ nm}} \sim 17 : 1$ in chloroform to $25 : 1$ in MeOH) of the latter.⁶² It should be noted that the contribution of the lower energy band in terms of absorbance is particularly high in chloroform. Hence, this could be due to some weak charge transfer operative in **5g**, which is somewhat dampened in solvents of higher polarity (THF, DMF and MeOH) due to the unequal stabilization of the ground and excited states. In water (pH 7.0), the absorption band lost its vibrational nature to some

Table 4 Important steady state spectral data of **5g**

Solvent	Abs. (nm)	Em (nm)/(ex 290 nm)	Stokes' shift (cm^{-1})
CHCl_3	290, 300, 360	350, 420	5911, 10 673
THF	290, 300, 350	350, 400	5911, 9483
DMF	290, 300, 350	350, 400	5911, 9483
MeOH	290, 300, 350	350, 400	5911, 9483
Water	290, 300	350, 420	5911, 10 673

extent, along with a broad tail spanning from 400 nm to $\sim 550 \text{ nm}$. This could be rationalized by considering the poor solubility of **5g** in water, possibly inducing the formation of aggregates in solution, which is reported to afford a Mie scattering-induced broad absorption tail.⁶³

Upon exciting **5g** at 300 nm (the most intense absorption band), some interesting emission spectral features were observed. The common feature in all solvents was the appearance of a structured band from 350–370 nm, typical of carbazole derivatives,⁶⁴ and a broad tail from 400–450 nm. One striking difference in chloroform was the presence of a very broad tail from 400 nm, and spanning through the spectral region of the experiment. The presence of a homogeneous electronic ground state was ensured by the following: (i) excitation-independent emission spectrum, and (ii) overlap of the excitation spectrum with the absorption spectrum (ESI, Fig. S1†).

From Fig. 2(B), it could be seen that the excitation spectrum of **5g** is broad with a significantly red-shifted excitation maximum ($\sim 350 \text{ nm}$). The solid-state emission spectrum is independent of the excitation wavelength, with a structured emission band with an emission maximum at 450 nm. The red shift in the absorption and emission spectra in the solid-state could be due to stabilization of the electronic states caused by non-classical interactions, as evidenced from the crystal structure analysis [Fig. 1(D)]. Structured bands observed in the solid-state form appear, contradicting the generally observed disappearance of vibrational bands in the solid-state emission spectra of organic fluorophores.^{65,66} However, this could also be the result of various types of aggregates (J, H, *etc.*), resulting in such an undulated nature of the emission spectrum or more

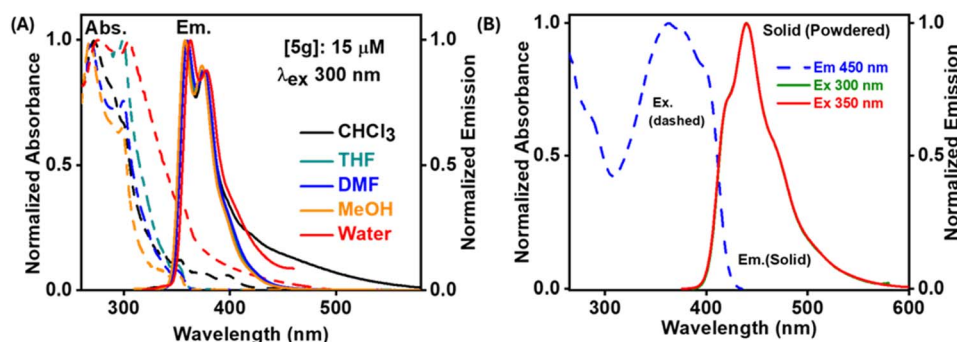


Fig. 2 (A) Steady-state absorption (dashed lines) and emission (solid lines) spectra of **5g** in various solvents, as indicated in the figure. The concentration was 15 μM and the excitation wavelength was 300 nm. (B) Steady-state absorption (dashed line) and emission (solid line) spectra of **5g** in the solid state. The excitation wavelength was 300 nm.



than one emitting species in the excited state, which could not be clarified from the steady-state emission spectrum. Thus, although the steady-state emission spectra in the solution and solid phase could provide useful information about the morphological behaviour of the emission spectra of **5g** in various states of aggregation, no concrete idea about the identity and number of emitting species could be obtained. Hence, the emission lifetime analysis was required to understand the photobehaviour of **5g**.

Time-resolved emission lifetime in solution and the solid phase

The emission lifetime of **5g** was recorded in various solvents and at various emission wavelengths (340 nm – 490 nm). Table 5 lists the emission lifetime parameters of **5g** in various solvents and in the solid state. The complete decays at various observed wavelengths are presented in the ESI (Fig. S2 and S3†), whereas the emission decays at 340 nm and 430 nm in various solvents, as well as the full emission decays at various observed wavelengths in the solid-state form are presented in Fig. 3(A)–(C), respectively. We first present a discussion on the solution phase, followed by the emission behaviour in the solid phase. In solution, upon excitation at 296 nm, the obtained emission decays [Fig. 3(A) and (B)] showed multi-exponential decay

Table 5 Excited state lifetime parameters of **5g** in various solvents. [$\alpha_{1,s}$] denotes the contribution to the excited state population. The error in estimation of the lifetimes is around 10%. Negative α denotes a growth component

State	λ_{obs} (nm)	τ_1 (ns)	α_1 (%)	τ_2 (ns)	α_2 (%)	τ_3 (ns)	α_3 (%)
CHCl ₃	340	—	—	2.3	95	12.0	5
	370	—	—		90		10
	400	—	—		80		20
	430	0.70	35		45		20
	460	0.70	80		10		10
	490	0.70	78		12		10
THF	340	—	—	0.8	75	8.0	25
	370	—	—		55		45
	400	—	—		47		53
	430	—	—		40		60
DMF	340	—	—	1.2	75	9.0	25
	370	—	—		70		30
	400	—	—		60		40
	430	—	—		59		41
MeOH	340	0.70	35	1.5	25	9.0	40
	370		25		40		35
	400		(–)100		80		120
	430		(–)100		85		115
Water	340	0.33	75	1.0	15	10.0	10
	370		55		30		15
	400		(–)100		80		120
	430		(–)100		70		130
Powder	350	0.20	70	1.2	25	17.0	5
	380		65		35		10
	410		60		25		15
	440		55		30		15
	470		(–)100		80		120
	500		(–)100		70		130

behaviour (Table 5). The common feature in all of the solvents was the presence of a sub-nanosecond to a few nanoseconds component ($\tau_1 = 0.8$ – 1.2 ns), and a long-lived component ($\tau_2 = 8.0$ – 12.0 ns). τ_1 had greater contribution in the blue region of observation, whereas τ_2 had greater contribution in the red region of observation (Table 5). In chloroform, methanol and water, an additional shorter component ($\tau_0 = 0.20$ – 0.70 ns) was required to provide a good fit to the emission decays (Table 5). In addition, in methanol and water, τ_0 decayed in the blue and rose in the red. The abnormally high value of the τ_2 component hints at an excimer-like emission, keeping in mind the structure-less red-shifted 400 nm emission band encountered in solution (*vide supra*), whereas the τ_1 component could be associated with emission from locally excited **5g** molecules. The rising nature of the τ_0 component directly proves a common channel between the monomer and the excimer species, and was strong evidence in favour of excimer emission, as observed for compounds showing excimer emission like naphthalene, pyrene and perylene.^{67–69} It should be noted that the excimer lifetime varies from one solvent to another, particularly in THF and DMF. The excimer emission lifetime changes with the polarity of the solvent in the case of molecules, where a $n \rightarrow \pi^*$ transition hampers the true value of the excimer lifetime.⁷⁰ The additional growth component in methanol and water could be explained by considering how the monomer-to-excimer formation is slowed down in protic solvents.⁷¹ Finally, the additional lifetime component in chloroform needed to be treated separately, as it was not a rising one. There was a considerably high contribution at the red region of observation in chloroform, apart from the fact that it had a significantly high lifetime. The fact that the time component does not show any rising nature outright negates the possibility of it being the time constant for the monomer \rightarrow excimer photoconversion. In addition, the very high contribution to the excited state population (35–78%, Table 5) signifies some other excited-state photo-event operative in chloroform, apart from excimer formation. At this juncture, the steady state spectral feature of **5g** in chloroform was revisited [Fig. 2(A)], which consisted of a considerably broad and red shifted tail with much higher Stokes' shift compared to that of the excimer band (Table 5). These two factors hinted at some excited state charge transfer event (ICT) in **5g**, which is the operative along with the excimer emission in chloroform, leading to the multi-exponential decay behaviour as observed.

In the solid state, the behaviour was like that observed in methanol and water, along with an abnormally high excimer lifetime of 17.0 ns [Fig. 3(C) and Table 5]. The excimer lifetime is particularly high due to the already existing packing and stacking in the solid state, as evidenced in the crystal structure discussion [Fig. 1(A) and (B)], which is reported to enhance the excimer lifetime.⁷² To explain photobehaviour in a concise manner, a photophysical scheme has been constructed and shown in Scheme 3.

In light of the literature reports^{48,49} and our previous work⁷³ on account of the activation of acetal, a plausible mechanism of the present study is depicted in Fig. 4. It was known that the acetal group can be activated by ferric chloride or other transition metal catalysts for the synthesis of heterocycles and other



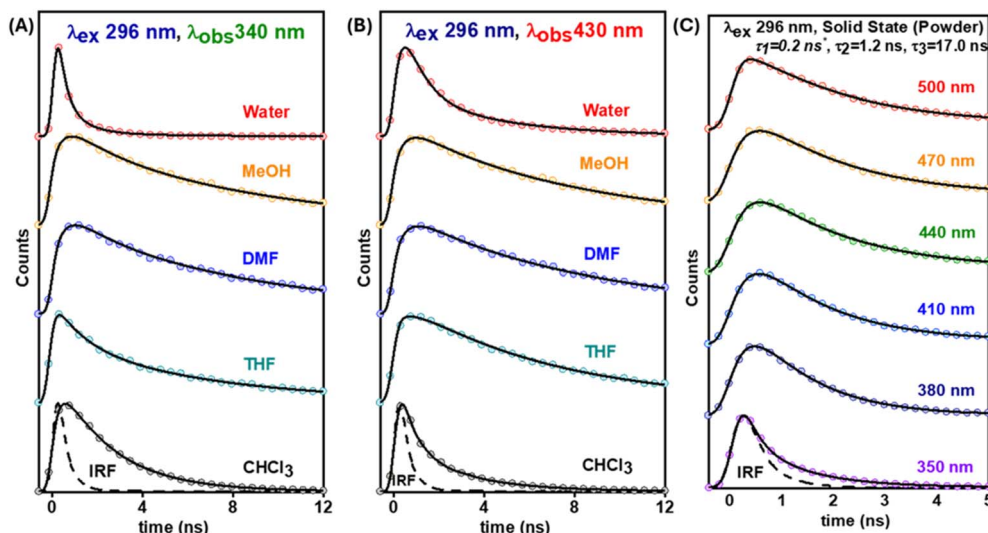
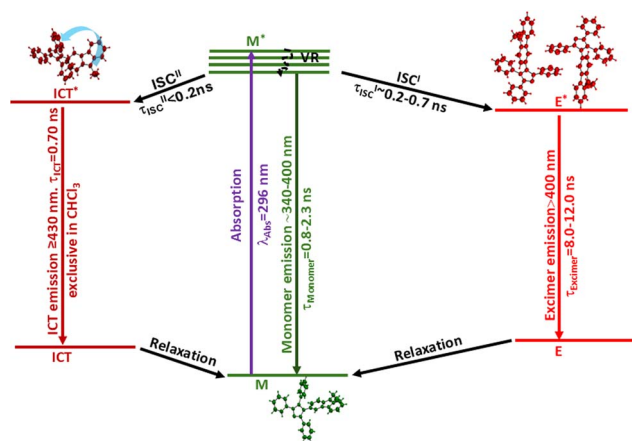


Fig. 3 Lifetime emission decays of **5g** in various solvents [(A and B) (15 μ M)] and solid states (C). The excitation and monitoring wavelengths are provided in the insets.



Scheme 3 Schematic of photophysical events in **5g** (not to scale). (The abbreviation of the terms are as follows: ISC = intersystem crossing, ICT = intramolecular charge transfer, E = excimer, and M = monomer).

functional materials under mild condition *via* C–O bond cleavage.^{48,49} Thus, we believe that iron of $\text{FeCl}_3/\text{SiO}_2$ coordinates with both oxygens of acetal and facilitated the formation of the intermediate oxonium ion (**B**) after expulsion of alkoxide ($\text{R}'\text{O}^-$) from (**A**). Then, ammonia/amine acts as a nucleophile to attack the highly reactive oxonium ion (**B**) to produce intermediate (**C**), which upon subsequent release of second $\text{R}'\text{O}^-$ by N-triggered elimination to produce imine (**D**). This reactive intermediate imine (**D**) invites a second molecule of ammonia/amine to participate in the nucleophilic addition reaction to afford aminal (**E**). This aminal then reacts with silica–ferric chloride-activated dione again to produce another imine (**F**), followed by ring closing to regenerate the catalyst and intermediate imidazolium cation (**G**). The release of the proton, following aromatization, yields imidazole **3** or **5** depending upon the stoichiometry of the ammonium acetate or amine

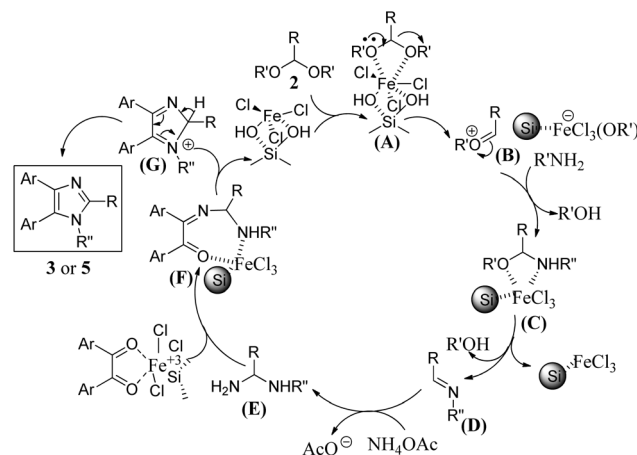


Fig. 4 Probable mechanism of the formation of **3** and **5**.

used. However, the involvement of the initial formation of any carbonyl compound *via* hydrolytic cleavage of acetal by the catalysis of FeCl_3 (ref. 74) is precluded, as evident from the NMR experiments. A solution of **2c** (10 mg) in DMSO-d_6 (0.6 mL) was taken in an NMR tube, then ^1H NMR spectra were recorded in the presence of $\text{FeCl}_3/\text{SiO}_2$ at ambient temperature after 30 min of shaking. No signal of the aldehydic functional group due to hydrolytic cleavage of the diethyl acetal group in **2c** was traced.

Conclusions

In conclusion, we have developed a benign catalytic system for the direct conversion to multisubstituted imidazoles by the reaction of acetals and benzils with ammonium acetate/amines as the source of nitrogen. The reaction occurred under mild conditions using $\text{FeCl}_3/\text{SiO}_2$ as the heterogeneous catalyst without the requirement of any toxic organic solvents. Novel



imidazole–carbazole hybrid compounds were also synthesised by adopting the present methodology. Single crystal X-ray diffraction studies indicated the presence of $\text{CH}\cdots\pi$ supramolecular interaction, which renders efficient molecular packing in the solid state. The steady state and spectro-dynamic investigation of one of the synthesized molecules having an imidazole–carbazole unit was investigated, and it was revealed that a solvent-dependent excimer-coupled ICT phenomenon guided the excited state photophysics. In the solid state, the compound showed an abnormally high excimer lifetime of about 17.0 ns. The investigation is ongoing in our group to suitably modify **5g** to drive the emission and absorption to the green-red region for subsequent studies on the biological imaging potential of the same class of compounds prepared in the current report.

Experimental section

General

^1H and ^{13}C NMR spectra were measured on a Bruker Ascend 400 spectrophotometer at ambient temperature using 400 MHz for ^1H and 100 MHz for ^{13}C . Chemical shifts were reported in parts per million from the tetramethyl silane and coupling constants were reported in hertz. Proton multiplicities were represented as s (singlet), d (doublet), dd (double doublet), t (triplet), q (quartet), and m (multiplet). FTIR spectra were recorded on a Bruker Alpha II FTIR spectrometer on neat or KBr pellets. Mass spectra (HRMS) were obtained from Orbitrap Exploris 120 (Thermo Scientific) using 70 eV in the positive ion mode. The single-crystal X-ray diffraction (XRD) data were collected on a Bruker D8 Venture system with a microfocus optics using $\text{Cu K}\alpha$ radiation. The data were analysed and processed with Bruker Apex III software suite 61 incorporated with multiple tools, such as cell_now and RLATT for the determination of the unit cell, SAINT-plus for data reduction, and SADABS for absorption correction. The structure solutions were performed with SHELXT, and the full-matrix least-squares refinements were performed with the SHELXL suite of programs incorporated in Olex 2.6. The steady-state absorption spectra were collected on a Shimadzu® UV-1900 absorption spectrophotometer. The steady-state emission spectra were collected in a Shimadzu RF-6000 emission spectrophotometer. Emission lifetime experiments were performed using a HORIBA® Jobin-Yvon TCSPC setup using a nano-LED light source of 296 nm ($\text{IRF} \sim 0.6$ ns). Emission lifetime data were deconvoluted and fitted using the DAS-6 software by HORIBA, which allows for individual and batch fits.

Materials

All reagents were purchased either from Sigma-Aldrich Chemical Co., USA, Acros Chemical Company, or SRL India, and were used as received unless otherwise specified. Commercially supplied petroleum ether (60–80 °C) and ethyl acetate were distilled before use. Column chromatography was performed on silica gel (60–120 mesh, 0.12–0.25 mm). Analytical thin-layer chromatography (TLC) was performed on 0.25 mm extra-hard silica gel plates with a UV254 fluorescent indicator. The silica-

supported ferric chloride reagent was prepared and stored as per the procedure previously described by us.⁴⁷

Synthesis

General procedure for the synthesis of tri and tetra-substituted imidazoles. A small glass vial was charged with the catalyst ($\text{FeCl}_3/\text{SiO}_2$) (20 mg, 2 mol% of FeCl_3), benzil (1.0 mmol), acetal (1.1 mmol), ammonium acetate (5.0 mmol) [for trisubstituted imidazoles] or ammonium acetate (2.5 mmol) and amine (2.5 mmol) [for tetra-substituted imidazoles], and then the mixture was heated at 100 °C until the full consumption of benzil (TLC). After completion of the reaction, the reaction mixture was diluted with EtOAc (5 mL), filtered, and the catalyst was washed with ethyl acetate. The combined filtrate was evaporated under vacuum. The desired product was isolated either by crystallization or by column chromatography using ethyl acetate–hexane (1 : 3 to 3 : 1).

Characterization data of the selected tri-substituted imidazoles

4,5-Bis(4-methoxyphenyl)-2-phenyl-1H-imidazole (3d). Yield: 90%, white solid, mp 170–172 °C [lit.⁷⁵ yellow oil]; IR (KBr) ν_{max} 2944, 2830, 1501, 1241, 1174 cm^{-1} ; ^1H NMR (400 MHz, CDCl_3) δ 7.86 (d, $J = 6.8$ Hz, 2H), 7.42–7.35 (m, 7H), 6.84 (d, $J = 8.0$ Hz, 4H), 3.81 (s, 6H); ^{13}C NMR (100 MHz, CDCl_3) δ 158.8, 145.6, 132.3, 130.0, 129.1, 128.7, 128.5, 125.4, 125.3, 113.9, 55.2; HRMS calcd for ($\text{C}_{23}\text{H}_{20}\text{N}_2\text{O}_2 + \text{H}^+$) 357.1603, found: 357.1591 ($\text{M} + \text{H}^+$).

2,2-Dimethyl-4,5-diphenyl-2H-imidazole (3h). Yield: 85%, white solid, mp 58–60 °C [lit.⁷⁶ brown oil]; IR (KBr) ν_{max} 3053, 2981, 2929, 1610, 1492, 1445, 1215, 801 cm^{-1} ; ^1H NMR (400 MHz, CDCl_3) δ 7.54–7.52 (m, 4H), 7.46 (t, $J = 7.6$ Hz, 2H), 7.37 (t, $J = 7.6$ Hz, 4H), 1.68 (s, 6H); ^{13}C NMR (100 MHz, CDCl_3) δ 164.2, 132.7, 130.2, 128.9, 128.3, 101.6, 24.2; HRMS calcd for ($\text{C}_{17}\text{H}_{16}\text{N}_2 + \text{H}^+$) 249.1392, found: 249.1434 ($\text{M} + \text{H}^+$).

Characterization data for the new tetra-substituted imidazoles (5)

1,2-Diphenyl-1H-phenanthro[9,10-d]imidazole (5f). Yield: 86%, white solid, mp 192–194 °C; IR (KBr) ν_{max} 1693, 1459, 1385, 1136, 919, 692 cm^{-1} ; ^1H NMR (400 MHz, CDCl_3) δ 8.92 (d, $J = 8.0$ Hz, 1H), 8.80–8.72 (m, 2H), 7.79–7.54 (m, 10H), 7.33–7.20 (m, 5H); ^{13}C NMR (100 MHz, CDCl_3) δ 151.0, 138.7, 137.4, 130.5, 130.1, 129.8, 129.5, 129.3, 129.1, 128.8, 128.3, 128.2, 128.1, 127.3, 127.2, 126.3, 125.6, 124.9, 124.1, 123.1, 123.1, 122.8, 120.9; HRMS calcd for ($\text{C}_{27}\text{H}_{18}\text{N}_2 + \text{H}^+$) 371.1548, found: 371.1538 ($\text{M} + \text{H}^+$).

9-Ethyl-3-(2,4,5-triphenyl-1H-imidazol-1-yl)-9H-carbazole (5g). Yield: 82%, white solid, mp 146–148 °C; IR (KBr) ν_{max} 3051, 2972, 1593, 1476, 1223, 1136, 1080, 923, 688 cm^{-1} ; ^1H NMR (400 MHz, CDCl_3) δ 7.96 (d, $J = 8.0$ Hz, 1H), 7.83 (s, 1H), 7.67 (d, $J = 8.0$ Hz, 2H), 7.53–7.50 (m, 3H), 7.44 (d, $J = 8.4$ Hz, 1H), 7.32–7.18 (m, 14H), 4.35 (q, $J = 7.2$ Hz, 2H), 1.46 (t, $J = 7.6$ Hz, 3H); ^{13}C NMR (100 MHz, CDCl_3) δ 147.3, 140.5, 139.1, 138.0, 134.7, 131.6, 131.1, 130.9, 130.8, 128.8, 128.6, 128.2, 128.1, 128.0, 127.7, 127.4, 126.5, 126.4, 125.9, 122.9, 122.4, 120.7, 120.4, 119.2, 108.8, 108.5, 37.7, 13.8; HRMS calcd for ($\text{C}_{35}\text{H}_{27}\text{N}_3 + \text{H}^+$) 490.2283, found: 490.2283 ($\text{M} + \text{H}^+$); HPLC (acetonitrile), $R_t = 14.188$ min, 100%.

Data availability

The data supporting this article are available as part of the supplementary information (ESI†). Crystallographic data for **5g** has been deposited at the Cambridge Crystallographic Data Centre (CCDC) under the deposition number 2361185 and can be obtained from <https://www.ccdc.cam.ac.uk> and <https://www.fiz-karlsruhe.de>.

Author contributions

S. M. designed the work. B. D. performed all experiments. A. B. contributed to the photophysical and lifetime measurement studies. B. P. and R. N. performed XRD studies and the processing of the X-ray data. S. M. and B. D. analyzed the spectral data, and wrote the manuscript with input from A. B. All authors reviewed and approved the final version of the manuscript.

Conflicts of interest

There are no conflicts to declare. The authors also declare that no funds, grants, or other support were received during the preparation of this manuscript.

Acknowledgements

We are grateful to the Department of Science and Technology, Govt. of India, for providing the 400 MHz NMR facility under DST-FIST (No. SR/FST/CSI-263/2015) and CIC, Tripura University for the instrumental facility. B. D. sincerely acknowledges Tripura University for providing the Non-NET fellowship.

Notes and references

- 1 B.-F. Ruan, Q.-L. Guo, Q.-S. Li, L.-Z. Li, G. S. Deora and B.-G. Zhou, *Curr. Top. Med. Chem.*, 2022, **22**, 578–599.
- 2 M. Yar, M. Bajda, S. Shahzad, N. Ullah, M. A. Gilani, M. Ashraf, A. Rauf and A. Shaukat, *Bioorg. Chem.*, 2015, **58**, 65–71.
- 3 A. Siwach and P. K. Verma, *BMC Chem.*, 2021, **15**, 12.
- 4 D. I. Ma Gee, M. Bahramnejad and M. Dabiri, *Tetrahedron Lett.*, 2013, **54**, 2591–2594.
- 5 A. Magyar and Z. Hell, *Synlett*, 2019, **30**, 89–93.
- 6 A. Reyes-Arellano, O. Gómez-García and J. Torres-Jaramillo, *Med. Chem.*, 2016, **6**, 561–570.
- 7 A. Verma, S. Joshi and D. Singh, *J. Chem.*, 2013, **2013**, 329412.
- 8 D. A. Shabalin and J. E. Camp, *Org. Biomol. Chem.*, 2020, **18**, 3950–3964.
- 9 I. B. A. Ghani, M. Khalid, M. I. Hussain, M. M. Hussain, R. Ashraf and J. Wang, *Mater. Sci. Semicond. Process.*, 2022, **148**, 106788.
- 10 M. Kumar, D. Kumar and V. Raj, *Current Synthetic and Systems Biology*, 2017, **5**, 1000135.
- 11 M. Y. Berezin, J. Kao and S. Achilefua, *Chemistry*, 2009, **15**, 3560–3566.
- 12 S. Zaman, K. Mitsuru and A. D. Abell, *Org. Lett.*, 2005, **7**, 609–611.
- 13 P. Koch, C. Bäuerlein, H. Jank and S. Laufer, *J. Med. Chem.*, 2008, **51**, 5630–5640.
- 14 E. M. Perchellet, J. P. Perchellet and P. W. Baures, *J. Med. Chem.*, 2005, **48**, 5955–5965.
- 15 G. Haberhauer and F. Rominger, *Eur. J. Org. Chem.*, 2003, 3209–3218.
- 16 A. Negi, J. M. Alex, S. M. Amrutkar, A. T. Baviskar, G. Joshi, S. Singh, U. C. Banerjee and R. Kumar, *Bioorg. Med. Chem.*, 2015, **23**, 5654–5661.
- 17 T. F. Gallagher, S. M. Fier-Thompson, R. S. Garigipati, M. E. Sorenson, J. M. Smietana, D. Lee, P. E. Bender, J. C. Lee, J. T. Laydon, D. E. Griswold, M. C. Chabot-Fletcher, J. J. Breton and J. L. Adams, *Bioorg. Med. Chem. Lett.*, 1995, **5**, 1171–1176.
- 18 C. Leister, Y. Wang, Z. Zhao and C. W. Lindsley, *Org. Lett.*, 2004, **6**, 1453–1456.
- 19 T. Yamamoto, T. Uemura, A. Tanimoto and S. Sasaki, *Macromolecules*, 2003, **36**, 1047–1053.
- 20 H. Konishi, T. Ueda, T. Muto and K. Manabe, *Org. Lett.*, 2012, **14**, 4722–4725.
- 21 V. G. Sree, C. Bathula, H.-K. Youi, H.-S. Kim, J. I. Sohn and H. Im, *J. Mol. Liq.*, 2021, **338**, 116708.
- 22 Y. Dong, J. Qian, Y. Liu, N. Zhu, B. Xu, C. L. Ho, W. Tian and W. Y. Wong, *New J. Chem.*, 2019, **43**, 1844–1850.
- 23 B. A. Omotowa and J. M. Shreeve, *Organometallics*, 2004, **23**, 783–791.
- 24 N. T. Zhang, C. C. Zeng, C. M. Lam, R. K. Gbur and R. D. Little, *J. Org. Chem.*, 2013, **78**, 2104–2110.
- 25 S. R. Nayak, S. Patel and S. Vaidyanathan, *New J. Chem.*, 2023, **47**, 3524–3534.
- 26 P. Bellotti, M. Koy, M. N. Hopkinson and F. Glorius, *Nat. Rev. Chem.*, 2021, **5**, 711–725.
- 27 N. A. Kukhta and M. R. Bryce, *Mater. Horiz.*, 2021, **8**, 33–55.
- 28 J. Gierschner, J. Shi, B. Milián-Medina, D. Roca-Sanjuán, S. Varghese and S. Park, *Adv. Opt. Mater.*, 2021, **9**, 2002251.
- 29 Y. Tan, Z. Zhao, L. Shang, Y. Liu, C. Wei, J. Li, H. Wei, Z. Liu, Z. Bian and C. Huang, *J. Mater. Chem. C*, 2017, **5**, 11901–11909.
- 30 X. Wang, J. Lin, H. Li, C. Wang and X. Wang, *RSC Adv.*, 2022, **12**, 4437–4445.
- 31 D. Kumar, D. N. Kommi, N. Bollineni, A. R. Patel and A. K. Chakraborti, *Green Chem.*, 2012, **14**, 2038–2049.
- 32 M. Chakraborty, B. Deb, B. Dey, S. A. Hussain, D. K. Maiti and S. Majumdar, *ChemistrySelect*, 2017, **2**, 241–245.
- 33 M. Antolini, A. Bozzoli, C. Ghiron, G. Kennedy, T. Rossi and A. Ursini, *Bioorg. Med. Chem. Lett.*, 1999, **9**, 1023–1028.
- 34 C. Mukhopadhyay and P. K. Tapaswi, *Green Chem. Lett. Rev.*, 2012, **5**, 109–120.
- 35 K. F. Shelke, S. B. Sapkal, G. K. Kakade, B. B. Shingate and M. S. Shingare, *Green Chem. Lett. Rev.*, 2010, **3**, 27–32.
- 36 X. L. Yu, Y. H. Fan, X. N. Zheng, J. F. Gao, L. G. Zhuang, Y. L. Yu, J. H. Xi and D. W. Zhang, *Molecules*, 2023, **28**, 4845.
- 37 H. Naeimi and D. Aghaseyedarimi, *New J. Chem.*, 2015, **39**, 9415–9421.
- 38 M. Nejatianfar, B. Akhlaghinia and R. Jahanshahi, *Appl. Organomet. Chem.*, 2017, **32**, e4095.
- 39 Z. Zarnegar and J. Safari, *New J. Chem.*, 2014, **38**, 4555–4565.



- 40 J. Mullaivendhan, I. Akbar, M. K. Gatasheh, A. A. Hatamleh, A. Ahamed, M. H. S. Abuthakir and R. Gurusamy, *BMC Chem.*, 2023, **17**, 155–170.
- 41 D. S. Weinstein, W. Liu, K. Ngu, C. Langevine, D. W. Combs, S. Zhuang, C. Chen, C. S. Madsen, T. W. Harper and J. A. Robl, *Bioorg. Med. Chem. Lett.*, 2007, **17**, 5115–5120.
- 42 C. F. Claiborne, N. J. Liverton and K. T. Nguyen, *Tetrahedron Lett.*, 1998, **39**, 8939–8942.
- 43 A. R. Siamaki and B. A. Arndtsen, *J. Am. Chem. Soc.*, 2006, **128**, 6050–6051.
- 44 M. Wang, L. Li, J. Lu, N. Luo, X. Zhang and F. Wang, *Green Chem.*, 2017, **19**, 5172–5177.
- 45 M. B. Gawande, R. Hosseinpour and R. Luque, *Curr. Org. Synth.*, 2014, **11**, 526–544.
- 46 S. Majumdar, A. Chakraborty, S. Bhattacharjee, S. Debnath and D. K. Maiti, *Tetrahedron Lett.*, 2016, **57**, 4595–4598.
- 47 B. Deb, S. Debnath, A. Chakraborty and S. Majumdar, *RSC Adv.*, 2021, **11**, 30827–30839.
- 48 T. Xu, Q. Yang, D. Li, J. Dong, Z. Yu and Y. Li, *Chem.–Eur. J.*, 2010, **16**, 9264–9272.
- 49 S. Ghosh, S. Khamarui, K. S. Gayen and D. K. Maiti, *Sci. Rep.*, 2013, **3**, 2987.
- 50 N. L. Higuera, D. Peña-Solórzano and C. Ochoa-Puentes, *Synlett*, 2019, **30**, 225–229.
- 51 S. Damavandi, *Heterocycl. Commun.*, 2011, **17**, 79–81.
- 52 S. S. Dipake, V. D. Ingale, S. A. Korde, M. K. Lande, A. S. Rajbhoj and S. T. Gaikwad, *RSC Adv.*, 2022, **12**, 4358–4369.
- 53 M. Waheed, N. Ahmed, M. A. Alsharif, M. I. Alahmdi and S. Mukhtar, *ChemistrySelect*, 2017, **2**, 7946–7950.
- 54 Y. Ran, M. Li and Z.-Z. Zhang, *Molecules*, 2015, **20**, 20286–20296.
- 55 A. C. Sedgwick, L. Wu, H. H. Han, S. D. Bull, X. P. He, T. D. James, J. L. Sessler, B. Z. Tang, H. Tian and J. Yoon, *Chem. Soc. Rev.*, 2018, **47**(55), 8842–8880.
- 56 S. Thazhathethil, T. Muramatsu, N. Tamaoki, C. Weder and Y. Sagara, *Angew. Chem., Int. Ed.*, 2022, **61**, e202209225.
- 57 Y. Chen, *Molecules*, 2022, **27**, 8628.
- 58 S. A. Bagnich, S. Athanasopoulos, A. Rudnick, P. Schroegel, I. Bauer, N. C. Greenham, P. Strohriegl and A. Köhler, *J. Phys. Chem. C*, 2015, **119**, 2380–2387.
- 59 C. Zhao, T. Schwartz, B. Stöger, F. J. White, J. Chen, D. Ma, J. Fröhlich and P. Kautny, *J. Mater. Chem. C*, 2018, **6**, 9914–9924.
- 60 C. Chen, K. C. Chong, Y. Pan, G. Qi, S. Xu and B. Liu, *ACS Mater. Lett.*, 2021, **3**, 1081–1087.
- 61 P. Naik, K. S. Keremane, M. R. Elmorsy, A. El-Shafei and A. V. Adhikari, *Electrochem. Sci. Adv.*, 2022, **2**, e2100061.
- 62 D. C. Harris and M. D. Bertolucci, *Symmetry and Spectroscopy: An Introduction to Vibrational and Electronic Spectroscopy*, Dover Publications, New York, 3rd edn, 1989.
- 63 G. S. He, W. C. Law, L. Liu, X. Zhang and P. N. Prasad, *Appl. Phys. Lett.*, 2012, **101**, 011110.
- 64 N. Guven and P. Camurlu, *J. Electrochem. Soc.*, 2015, **162**, H867–H876.
- 65 T. Schillmöller, P. N. Ruth, R. Herbst-Irmer and D. Stalke, *Chem.–Eur. J.*, 2020, **26**, 17390–17398.
- 66 J. L. Song, C. Lei and J. G. Mao, *Inorg. Chem.*, 2004, **43**, 5630–5634.
- 67 K. Uchida, M. Tanaka and M. Tomura, *J. Lumin.*, 1979, **20**, 409–414.
- 68 D. Ray Chawdhury, S. Narayanan, T. Agrawal and P. B. Bisht, *J. Lumin.*, 2023, **263**, 120084.
- 69 H. Yoo, J. Yang, A. Yousef, M. R. Wasielewski and D. Kim, *J. Am. Chem. Soc.*, 2010, **132**, 3939–3944.
- 70 E. Sebastian, J. Sunny and M. Hariharan, *Chem. Sci.*, 2022, **13**, 10824–10835.
- 71 G. Xie, Y. Sueishi and S. Yamamoto, *J. Fluoresc.*, 2005, **15**, 475–483.
- 72 X. Shan, W. Chi, H. Jiang, Z. Luo, C. Qian, H. Wu and Y. Zhao, *Angew. Chem.*, 2023, **62**(72), e202215652.
- 73 S. Majumdar, M. Chakraborty, D. K. Maiti, S. Chowdhury and J. Hossain, *RSC Adv.*, 2014, **4**, 16497–16502.
- 74 S. E. Sen, S. L. Roach, J. K. Boggs, G. J. Ewing and J. Magrath, *J. Org. Chem.*, 1997, **62**(19), 6684–6686.
- 75 L.-M. Recnik, M. A. El Hameid, M. Haider, M. Schnürch and M. D. Mihovilovic, *Synthesis*, 2013, **45**, 1387–1405.
- 76 X.-L. Wu and L. Dong, *Org. Lett.*, 2018, **20**, 6990–6993.

